Annu. Rev. Phys. Chem. 1996. 47:495–525

EXPERIMENTAL STUDIES OF RESONANCES IN UNIMOLECULAR DECOMPOSITION

Scott A. Reid
Department of Chemistry, Marquette University, Milwaukee, Wisconsin 53233

Hanna Reisler
Department of Chemistry, University of Southern California, Los Angeles, California 90089-0482

KEY WORDS: photodissociation dynamics, statistical processes, HCO, HFCO, CH_3O

ABSTRACT

In recent years we have witnessed tremendous progress in our understanding of unimolecular reactions on a fully state-resolved level. Here we describe recent state-resolved experimental studies of resonances in unimolecular reactions, focusing on the transition from isolated to overlapping resonances. Depending on the well depth and extent of intramolecular vibrational energy redistribution, the resonances can exhibit properties ranging from mode- and state-selective to statistical behavior. In the statistical limit the resonances are usually overlapped, and interference effects may become prominent. We use recent studies of HCO, HFCO, and CH_3O to examine the transition from mode-selective to statistical behavior in the isolated regime. Experimental and theoretical studies of NO_2, including photofragment yield spectra, fully resolved NO quantum state distributions, and decomposition rates are used to examine unimolecular decomposition in the regime of overlapping resonances.

INTRODUCTION

Resonances are important features of many fields in chemistry and physics, including nuclear reactions (1, 2), electron-atom and electron-molecule scattering (3, 4a–d), photoionization (3–5), molecular photodissociation (6, 7), and atom-molecule or bimolecule scattering (3, 8a,b). In nuclear physics, for example, the role of resonances in the decomposition of a compound nucleus has

0066-426X/96/1101-0495$08.00

long been recognized (1, 2, 9). In the 1960s, Ericson (10a,b) predicted that interferences resulting from overlap between resonances would cause spectra obtained for different final states to fluctuate with respect to line positions, shapes, and intensities. These predictions were later verified experimentally and the phenomenon is now known as Ericson fluctuations (10a,b).

Work on resonances and interference in their couplings to continua later inspired Mies & Krauss to apply the resonant scattering approach to unimolecular decomposition rates (11). They demonstrated that upon averaging over thermal initial conditions (typical of early activation experiments), interference effects were washed out and the averaged rates agreed with thermal rates obtained from statistical theories (11). Recently, it has become possible to extend the state-to-state experimental methods used to characterize direct photodissociation to study reactions proceeding via complex intermediates with deep potential wells. As the well depth increases, so does the importance of intramolecular vibrational energy redistribution (IVR) and overlapping resonances, until the fully ergodic limit best described by statistical theories is reached. However, at a quantum dynamical level, these chaotic systems are described by distinct resonances that undergo interference and exhibit fluctuations. The fluctuations arise from the evolution of wave functions representing random but specific nuclear motions directing them toward the transition state (TS) and on to final products.

Quantum state–resolved experiments have provided insights into the connection between resonance scattering and statistical behavior, and it is the purpose of this review to examine recent advances in this area. Excellent reviews of theoretical studies of this subject have recently appeared (12a–c), and therefore we limit ourselves to experimental investigations. We have chosen systems that highlight the decomposition of molecules exhibiting (*a*) isolated resonances that can be assigned normal or local mode (i.e. zero-order) labels (e.g. HCO), (*b*) isolated resonances with increasing degree of IVR up to the chaotic limit (e.g. HFCO, CH_3O), and (*c*) overlapping resonances in the chaotic regime (e.g. NO_2). Our goal is not to provide an exhaustive review; rather, the choice of molecules is dictated by the wish to best illustrate specific themes of this review and to avoid systems that have been recently reviewed. The reader is encouraged to peruse reviews and original articles describing the detailed and insightful state-to-state studies of the unimolecular decomposition of molecules such as H_2CO (13a–21), NCNO (22–27), H_2O_2 (28–37), HN_3 (38–41), and CH_2CO (13a,b, 42–49) that created much of the foundation needed for the understanding of the issues discussed here.

In the absence of additional line-broadening mechanisms, the spectrum of an isolated resonance (or discrete state embedded in and coupled to a dissociation continuum) shows a Lorentzian line shape of width $\Gamma = (2\pi c\tau)^{-1}$, where τ is

the resonance lifetime. The resonances are isolated if the average energy width Γ is much smaller than the inverse level density ρ^{-1}, i.e. $\Gamma\rho \ll 1$. We also consider isolated neighboring resonances that overlap but are coupled to different and noninteracting continua (50). An isolated resonance is characterized by (*a*) its energy, E_R, which reflects the inner or bound region of the potential energy surface (PES); (*b*) its width, Γ_R, which uniquely specifies the resonance lifetime and is determined by the coupling strength to the continuum; and (*c*) the quantum state distributions of the product(s), which reflect scattering from the resonance to the product states via the TS. Each resonance has a unique width and is associated with a unique final state distribution; however, when discussing the discrete states that are coupled to the continuum, it is common to refer to the extent of IVR that controls mode-specific vs statistical behavior (51, 52). For mode-specific behavior, the resonances can be assigned unique quantum numbers by using a zero-order Hamiltonian and basis set (51), and the resonance widths and final state distributions show a systematic dependence on these labels. In contrast, the statistical case embodies random rather than systematic dependences (52), since resonance assignments are possible only in terms of rigorously conserved labels, i.e. total angular momentum (*J*), parity, and rovibronic symmetry. As examples of isolated resonances in unimolecular reactions, we describe recent state-resolved studies of HCO, HFCO, and CH_3O that cover the range from negligible to significant IVR.

The resonance widths are typically determined from total or partial absorption spectra [the so-called photofragment yield (PHOFRY), photofragment excitation (PHOFEX), or action spectra]. In this method (13a,b, 26a,b, 53), molecules are optically excited to energies in excess of the dissociation threshold, and nascent fragments are then detected state selectively. The final state-selected spectra reflect probabilities both for absorption and dissociation into the monitored fragment state (6). For an isolated resonance, the partial and total absorption spectra show identical Lorentzian line shapes (6). The peak intensity in each partial spectrum reflects the branching ratio for that product state, i.e.

$$\sigma(E, f) = \sigma_{\text{tot}}(E)\frac{\Gamma_f}{\Gamma}. \quad 1.$$

In Equation 1 the total decay width Γ is the sum of partial widths Γ_f for each product state *f*:

$$\Gamma = \sum_f \Gamma_f. \quad 2.$$

Note that for an isolated resonance in the weak coupling limit the final state distribution is constant across the absorption line (6).

In contrast, when neighboring resonances overlap and couple to a common continuum, interference can modify line positions, shapes, and widths, giving

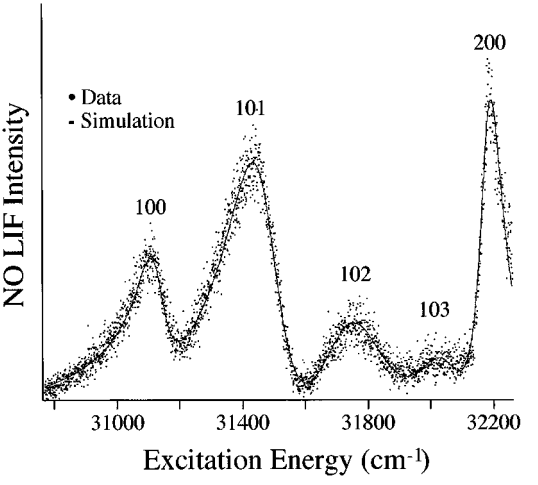

Figure 1 Photofragment yield (PHOFRY) spectrum of jet-cooled FNO in the region of the $S_1(10\nu_3) \leftarrow S_1(000)$ transition. The dots represent the experimentally determined yield of a specific NO quantum state, $v = 1$ and $J = 41.5$, as a function of photolysis laser frequency. The solid line is the sum of individual fits of each feature to a Fano line shape function.

rise to asymmetric line shapes commonly known as Fano profiles (54). For an illustrative example, consider the case of a single resonance embedded in a continuum in which interference arises as a result of simultaneous excitation of the resonance and continuum, as recently observed in the photodissociation of FNO (55, 56). Figure 1 shows a $S_1 \leftarrow S_0$ state-specific PHOFRY spectrum of jet-cooled FNO; note the marked asymmetry of several of the absorption features. Although in this case the resonances overlap, they interact only weakly, and the spectrum can be simulated by a simple (incoherent) superposition of five Fano line shape functions (4b, 54–61), each characterized by an asymmetry parameter, q. Note that q is signed, and a feature appears asymmetric when q is near, but not equal to, zero. For large q (≥ 10) a feature appears Lorentzian.

The source of the asymmetric line shapes observed in Figure 1 is revealed by time-dependent calculations on a two-dimensional PES (fixed ∠FNO), which show that optical excitation accesses the region near a small barrier to dissociation on the S_1 surface, which has a shallow well (58a,b). Following excitation, the initial wave packet splits into two parts: One is temporarily trapped in the well, while the other exits directly on the repulsive side of the barrier. It is the interference between these direct and indirect paths that leads to asymmetric line shapes in the frequency domain. Such interference can produce a marked final state dependence of the resonance line shapes. For FNO the resonance

line shapes change very little for different J levels within the same vibrational level (57). However, marked changes are observed for levels of the same J in different vibrational manifolds (Figure 2). Here the resonance width is similar in the two spectra displayed in each panel, but the q parameter reverses sign, although it is of similar magnitude. The final state dependence of the line shapes is also seen in dynamical calculations (59, 60).

Figures 1 and 2 show that interference between individual resonances and continua can produce both non-Lorentzian line shapes and a marked final state dependence of the line shape in PHOFRY spectra. In this example the resonances overlap but interact only weakly. Consider now the case of interacting overlapping resonances, i.e. overlapping resonances coupled to the same continuum (50). If the final states are uncorrelated, each may derive from a different combination of resonance amplitudes and phases, giving rise to different interference patterns. Thus, the PHOFRY spectra for different final states may show markedly different line positions, shapes, and widths, as indeed has been recently observed in state-specific PHOFRY spectra of NO_2 (62–67) (Figure 3). Asymmetric line shapes that result from interference among overlapping resonances were first observed by Moore and coworkers in Stark level-crossing spectra of D_2CO (13b). Here, we focus primarily on recent experimental and theoretical studies of NO_2 above dissociation threshold (D_0) that aid in understanding unimolecular decomposition in the regime of overlapping resonances.

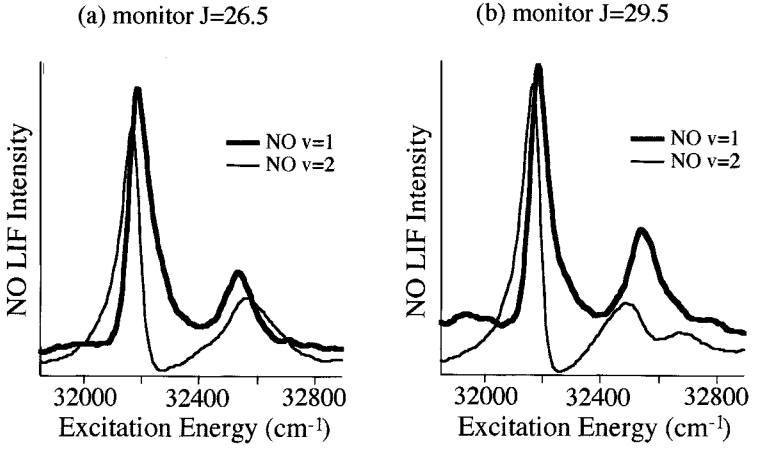

Figure 2 Photofragment yield (PHOFRY) spectrum of jet-cooled FNO in the region of the $S_1(200) \leftarrow S_1(000)$ transition. The two panels show spectra obtained for specific NO quantum states with the same total angular momentum ($J = 26.5$ or 29.5) but different quanta of vibrational excitation ($v = 2$ vs $v = 1$). Note the marked change in the resonance line shape between the two spectra in each panel.

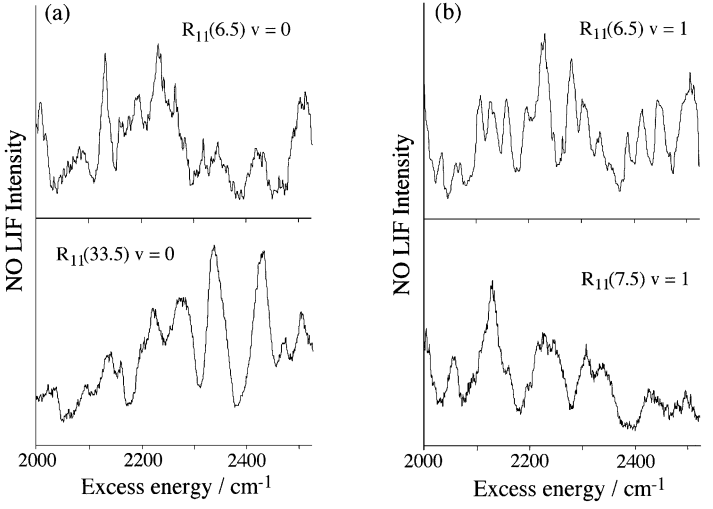

Figure 3 Representative NO_2 infrared (IR)-visible PHOFRY spectra at an excess energy $E^\dagger$ = 2000–2500 cm^{-1} that were obtained by monitoring NO levels with the same quanta of vibrational excitation but (*a*) of significantly different *J* and (*b*) of similar *J*. Note the marked change in peak intensities, shapes, and widths between the two spectra in each panel.

EXPERIMENTAL METHODOLOGIES

State-resolved studies require both reactant and product quantum state selection. The latter is readily achieved for selected fragments via laser-induced fluorescence (LIF) or resonance-enhanced multiphoton ionization (REMPI) detection, e.g. complete quantum state specification is possible for a diatom such as NO (68, 69). For preparation of reactants in specific quantum states with total energy in excess of reaction threshold, the combination of expansion or jet-cooling (70), which in principle allows the selection of a single (i.e. the energetically lowest) state of the unexcited reactant, and double-resonance excitation via methods such as stimulated emission pumping (SEP) (71–75) and infrared (IR)-visible double resonance (36, 37, 62, 64, 65a,b, 76, 77) (Figure 4) is particularly powerful. For example, our studies of NO_2 (62, 64, 65a,b) feature a combination of jet-cooling and double-resonance IR-visible excitation (Figure 4*b*), in which specific rotational states in the (101 $\leftarrow$ 000) band are excited with tunable IR radiation from a $LiNbO_3$ optical parametric oscillator (OPO), and the vibrationally excited molecules are further excited with a tunable laser to energies above D_0.

As evident from the studies reviewed here, SEP is a powerful tool for the study of high-lying vibrational states of polyatomic molecules (71–75). In the

traditional implementation, fluorescence dip–detected SEP (FD-SEP) (71–75) "dump" transitions are detected as depletions in the spontaneous fluorescence from the "pump" laser-prepared excited state. Recently, background-free SEP variants based on resonant four-wave mixing (RFWM) have been developed (78–82). The RFWM-SEP methods typically feature nonlinear scaling in both sample number density and the optical cross sections of the pump and dump transitions and are less general than FD-SEP (81, 82). However, the RFWM-SEP methods are less susceptible to saturation broadening and thus provide more accurate line width measurements (81, 82). Other new experimental techniques for obtaining total absorption or absorption-like spectra of dissociative molecular states include fluorescence dip–detected optical-optical double resonance (83, 84); variants of the RFWM technique, such as degenerate four-wave mixing (85–87) and laser-induced grating (88–90) spectroscopies; and cavity ring-down spectroscopy (91). At present only a few applications of these methods to the spectroscopy of dissociative states have been reported (83–89);

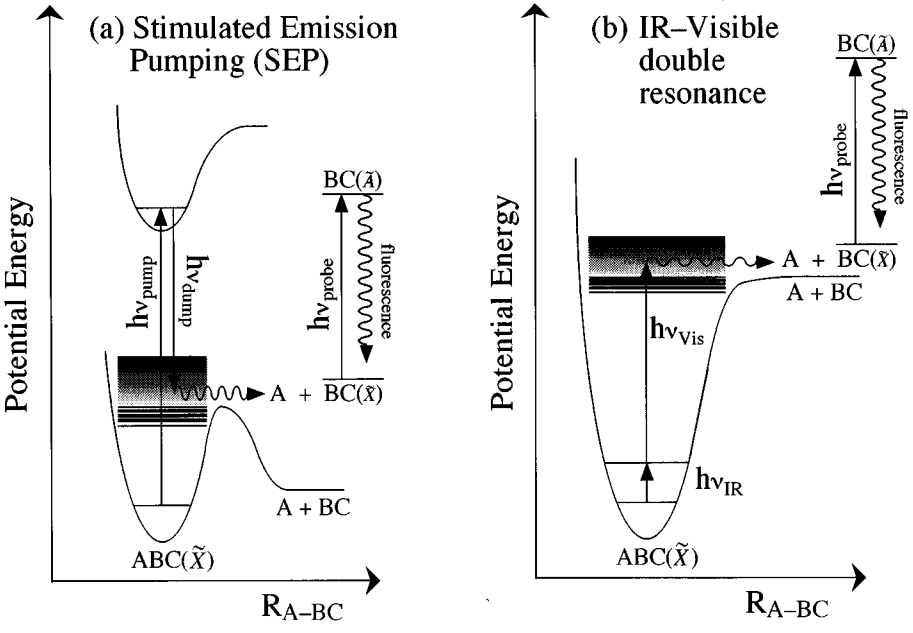

Figure 4 Schematic illustration of the state-selected unimolecular reaction of a triatomic molecule initiated via double-resonance optical excitation with (*a*) stimulated emission pumping (SEP) and (*b*) IR-visible double resonance. Following reaction, the quantum state distribution of the diatomic fragment is interrogated via LIF.

however, these techniques and their variants will surely profoundly impact the study of resonances in photofragmentation.

In the case of double-resonance excitation, PHOFRY or product-detected stimulated emission (PDSE) spectra are obtained by scanning the photolysis (dump in PDSE) wavelength for fixed preexcitation (pump) and probe wavelengths (62, 64, 65a,b, 92). In our studies of NO_2, such spectra are used to deduce information on thermal averaging through comparisons with spectra obtained via one-photon excitation under similar experimental conditions (63–65b). Although PHOFRY or PDSE spectra inherently contain information on the quantum state distribution of the fragments, these distributions are usually obtained by fixing the excitation wavelength(s) and scanning the probe laser to detect products in specific quantum states (e.g. vibrational, rotational, spin-orbit, Λ-doublet). Quantum state populations can be extracted from the experimental intensities via knowledge of the relevant Franck-Condon and Hönl-London factors, accounting for fragment alignment ($\mu - J$ correlation) in the case of fast reactions (93).

ISOLATED RESONANCES IN UNIMOLECULAR REACTIONS: FROM MODE-SPECIFIC TO STATISTICAL BEHAVIOR

The unimolecular reactions of HCO, HFCO, and CH_3O provide excellent opportunities to examine unimolecular decomposition in the regime of isolated resonances. Their dissociative ground PESs feature small threshold energies for reaction ($\sim$ 20–50 kcal/mol), and the level density in the region near and above the reaction barrier is thus sparse, which calls into question the applicability of statistical theories such as the Rice-Ramsperger-Kassel-Marcus (RRKM) theory to their reactions. Experimentally, the use of SEP (Figure 4) and its variants has allowed the study of levels below as well as above the reaction barrier in all three systems.

HCO: Isolated Resonances with Specific Normal (Local) Mode Labels

Numerous experimental studies have probed the ground PES of the HCO radical (81, 82, 94–110). Owing to pronounced Franck-Condon activity in the carbonyl stretching and bending modes, single vibronic level–dispersed fluorescence (SVLDF) and SEP spectra obtained following excitation in the $\tilde{B} \leftarrow \tilde{X}$ system have provided the most global characterization (81, 82, 103, 106–110). High-resolution SEP measurements have been made by several groups (81, 82, 107–110). Field and coworkers examined the energies and widths of 16 bound

and resonance states in the range 3,700–12,000 cm^{-1} above the $\tilde{X}$ state vibrationless level (107), while Houston and coworkers probed 8 resonances in the range 10,800–15,920 cm^{-1} and also reported nascent CO quantum state distributions (108–110). Most recently, Rohlfing and coworkers used both FD- and RFWM-SEP to characterize the energies and widths of 73 bound and resonance states (81, 82).

The unimolecular reaction of HCO is a clear, illustrative example of mode- and state-selective decomposition, particularly the striking dependence of the resonance widths on the normal mode quantum numbers (ν_1, ν_2, ν_3) (81, 82, 107–110). The narrowest widths, and thus longest lifetimes, are found for the pure carbonyl stretching states (0, ν_2, 0), which display distinctly nonmonotonic changes as a function of energy and are still rather narrow even at high energies (Figure 5) (82). The addition of bending excitation to these levels, i.e. excitation of the states (0, ν_2, ν_3), changes the width little at low ν_2 but increases the width at high ν_2 (82). Plots of resonance width versus ν_2 display pronounced structure in all observed progressions (82). The broadest resonances found contain excitation in the reaction coordinate (C-H stretch) (82).

The nascent quantum state distributions of the CO fragment also exhibit remarkable mode and state specificity (109, 110). The CO rotational state distributions are nonstatistical and highly structured, and their overall shapes are qualitatively similar to those observed in other CO elimination reactions with pronounced exit-channel barriers (111–113). The structure displays a marked dependence on both the vibrational (ν_1, ν_2, ν_3) and rotational quantum numbers (N, K_a, K_c) of the resonance state. In addition, the nascent CO vibrational state distributions are consistently inverted (110).

These studies provide detailed experimental data bases that can now be compared with state-of-the-art calculations, as evidenced by the extensive theoretical activity aimed at determining the resonance energies, widths, and CO quantum state distributions (114–129). Detailed comparisons between experiment and theory for the HCO system can be found elsewhere (12c, 82, 110, 128) and will not be described in detail; however, we note that both time-independent (114–125, 129) and time-dependent (126, 127) quantum mechanical calculations on ab initio PESs (114, 128) show trends in the resonance line widths that are consistent with the experimental findings. Structured CO rotational and inverted CO vibrational distributions have also been predicted by theory (127). These successes depend to a large extent on the accuracy of the PESs, and underscore the necessity of detailed knowledge of the PES in modeling mode- and state-specific decomposition.

Similar studies of the formyl isotopomer DCO have recently begun (130, 131). Rohlfing and coworkers obtained the energies of 112 bound and resonance

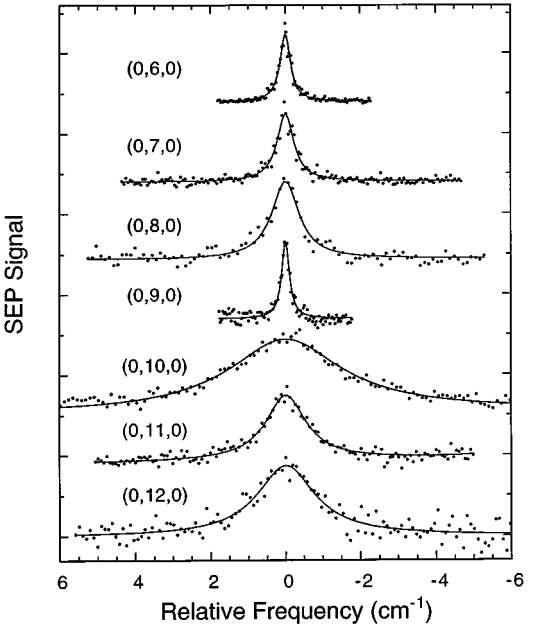

Figure 5 SEP spectra of a series of pure carbonyl stretching states (0, ν_2, 0) of HCO. In each spectrum the dump transition terminates on a single rotational state, 1_{01}, and the peak heights in each spectrum are normalized to the same value. The dots represent the experimental data; the solid lines are fits to single Lorentzian functions. The (0, 6, 0), (0, 7, 0), and (0, 8, 0) spectra were obtained using RFWM-SEP; all others via FD-SEP. (Reprinted from Reference 82, with permission of the authors.)

states of DCO ($\tilde{X}$) from SVLDF spectra (130). A complex polyad structure was observed because of near resonances among the vibrational mode frequencies (i.e. $\nu_1 \simeq \nu_2 \simeq 2\nu_3$); however, zeroth-order vibrational assignments were successfully made for 99 of the observed levels. High-resolution SEP measurements will supply detailed information on the resonance energies and widths (131) for comparisons with the detailed theoretical studies recently reported (12c, 125, 132).

HFCO: Isolated Resonances in a Regime of Restricted IVR

In their studies of HFCO (92, 113, 133–137), Moore and coworkers reported the first use of SEP to initiate unimolecular decomposition. Franck-Condon activity in the carbonyl stretching and out-of-plane bending modes in the $S_1 \leftrightarrow S_0$ electronic transition allows access via SEP to isolated metastable levels well above the ground state dissociation barrier ($\sim$17,200 cm^{-1}) to

HF + CO products. Strong mode specificity is observed in IVR in the dissociative region; in particular, high overtone levels of the out-of-plane bending mode display remarkable stability against IVR (136). This system is thus intermediate between HCO, where unique zeroth-order assignments are possible for almost all observed resonances, and CH_3O, where extensive IVR prohibits such assignments.

While the coupling of a discrete state to a dissociative continuum necessarily broadens the discrete absorption line, it may be impossible in a weak coupling regime such as the tunneling regime in HFCO and CH_3O (see below) to deconvolve the homogenous line width from other broadening mechanisms (laser bandwidth, Doppler broadening, etc). To circumvent this difficulty, Moore and coworkers used a triple-resonance pump-dump-probe scheme to determine lifetimes of isolated rovibrational levels 14,563–17,319 cm^{-1} above the vibrationless level (137). Striking mode and state specificity was observed on the basis of rotational level and vibrational symmetry. For a given vibrational level, increasing the J and K quantum numbers from 0 and 0 to 4 and 2, respectively, increased the reaction rate by up to two orders of magnitude! This remarkable behavior was explained as arising from Coriolis-induced coupling of the optically active level, itself only weakly coupled to the reaction coordinate, to levels containing significant excitation in that coordinate. These studies also produced the first observation of symmetry-induced mode specificity, an effect predicted by Miller in 1983 (138). For $J = 0$, rates for vibrational levels of A'' versus A' symmetry were smaller by a factor of ~ 20 (137), reflecting the requirement that A'' levels contain at least one quantum of out-of-plane bending excitation (see below).

At energies in excess of the dissociation barrier ($E > 17,150$ cm^{-1}) the coupling strength to the continuum rapidly increases, and the line widths are dominated by homogeneous broadening. Here line width measurements from high-resolution SEP spectra yielded dissociation rates for isolated resonances located 17,823–22,537 cm^{-1} above the vibrationless level (137). Many of these resonances are localized, i.e. can be uniquely assigned zeroth-order quantum numbers, and significant mode and state specificity is observed in the line widths. At a given energy, levels containing more quanta of excitation in the out-of-plane bending mode dissociate more slowly, reflecting the weak coupling of this motion to the in-plane reaction coordinate. The rotational state dependence of the dissociation rates was found to be weaker in the higher energy region. Recently, Choi & Moore (113) reported nascent CO quantum state distributions. The CO rotational state distributions are nonstatistical, peaking at $J = 45$–50 depending on the resonance excited, but their overall shapes are qualitatively similar to other CO elimination reactions with pronounced exit-

channel barriers (109–112). In contrast to HCO, a preference for CO($v = 0$) is observed, with $\sim$ 10% yield of vibrationally excited CO product.

Several theoretical studies have examined the HFCO reaction (139–144). The TS geometry was found to be planar in ab initio calculations (139–144), and a modified impulsive model was successfully used in concert with the ab initio TS geometry to rationalize the observed CO product state distributions (113). A calculation of vibrational mode couplings along the reaction coordinate using a reaction path Hamiltonian (144) showed that the out-of-plane bend is indeed the most weakly coupled mode (140). It is intriguing to note that despite the small size of this molecule and the relatively low reaction barrier, comparisons with RRKM theory displayed significant deviations only in the tunneling regime and for levels of low J (137), where IVR was found to be incomplete. By applying RRKM theory to model dissociation rates for high rotational states where Coriolis-induced mixing is operative, Choi & Moore derived a barrier height consistent with ab initio calculations (137).

CH_3O: Isolated Resonances in the Regime of Statistical Behavior

The methoxy radical (CH_3O) is an excellent system for examining IVR and its relationship to statistical theories of unimolecular reaction. In a series of detailed studies, Temps and coworkers have examined the spectroscopy and dynamics of the ground PES (145a–150). SVLDF spectra obtained following excitation of the $\tilde{A} \leftarrow \tilde{X}$ system show a pronounced progression in the carbonyl stretching mode (ν_3), allowing access via SEP to regions of the ground state potential up to $\sim$12,000 cm^{-1} above the vibrationless level, which is considerably in excess of the threshold energy for H-H_2CO bond fission E_0(H-H_2CO) $\simeq$ 8400 cm^{-1}. Resonance lifetimes in the tunneling regime, $\sim$ 7500 cm^{-1} above the vibrationless level, were determined via the triple-resonance pump-dump-probe scheme. In contrast to HCO and HFCO, extensive IVR prohibits full quantum state assignments of the resonances in this region (146, 148–150). However, the strict SEP selection rules allow the study of resonances well characterized in terms of rigorously conserved labels. Time-resolved decay profiles were recorded for six such resonances—the observed rate constants were found to vary over a factor of 30 for resonances separated in energy by only several cm^{-1} (146)! However, rate constants averaged over several resonances were in reasonable agreement with a RRKM calculation that included tunneling (146, 150).

At energies in excess of the dissociation barrier ($E \simeq$ 10,000 cm^{-1}) line width measurements from high-resolution SEP spectra were used to infer dissociation rates of isolated resonances (149, 150). Marked fluctuations in line width for energetically close resonances were observed; however, rate constants averaged over several resonances were in reasonable agreement with RRKM calculations

(149, 150). We note that strong fluctuations in single-resonance lifetimes have also been observed in Stark-level crossing studies of H_2CO by Moore and coworkers (13a,b, 16, 17a,b), where the average behavior is also consistent with RRKM predictions. These studies, which have been extensively reviewed elsewhere (13a), together with those of Temps and coworkers provide a beautiful illustration of the statistical fluctuations in state-specific resonance lifetimes that are a signature of the random coupling of individual molecular eigenstates to the continuum in the chaotic regime. To date, no information on the product quantum state distributions is available for the methoxy system.

NO_2 DECOMPOSITION: A CASE OF OVERLAPPING RESONANCES

Unimolecular reactions that can be described by statistical theories such as the RRKM theory are typically characterized by overlapping, rather than isolated, resonances (65a,b). Recently, experimental manifestations of overlapping resonances have been revealed in the state-to-state unimolecular reactions of H_2CO (13a,b) and NO_2 (62–67). Such studies require good initial and final state selection, a condition that is best met for small (triatomic) molecules. On the other hand, to justify comparisons with statistical theories the parent eigenstates must be ergodic (i.e. IVR should be complete), a condition not easily met for triatomic molecules (consider HCO, for example). NO_2 represents the unusual case in which all these conditions are satisfied.

The barrierless unimolecular reaction of NO_2 has been studied in detail as a function of excess energy [$D_0 = 25{,}130 \pm 2\ \mathrm{cm}^{-1}$ (66a,b, 89, 151)]:

$$\mathrm{NO_2}(E^\dagger) \rightarrow \mathrm{NO}\left(^2\Pi_\Omega;\, v;\, J;\, \Omega = 1/2, 3/2;\, \Lambda = A', A''\right) + \mathrm{O}\left(^3\mathrm{P}_j;\, j = 2, 1, 0\right),$$

where Ω and Λ are the NO spin-orbit and Λ-doublet states, respectively. Here, each state-selected NO product is correlated with up to three states of the O(^{3}P) fragment. Experimental studies include measurements of (*a*) unimolecular reaction rates of monoenergetic samples (152–158) and (*b*) detailed product state distributions (PSDs) including vector properties and correlated distributions (62–67, 88, 89, 151, 159–181). As a consequence of a strong nonadiabatic interaction in NO_2 promoted by the asymmetric stretching mode, a conical intersection of the optically accessible $^2B_2$ and ground $^2A_1$ surfaces occurs near the $^2B_2$ minimum (182–206). This interaction causes the extreme complexity of the NO_2 visible absorption spectrum and leads to vibronic chaos at excitation energies $> 16{,}000\ \mathrm{cm}^{-1}$ and rovibronic chaos near D_0 (201–206). It has been shown that eigenstates in the vicinity of D_0 are predominantly of $^2B_2/^2A_1$

character, while density of state considerations dictate that these eigenstates have a predominantly ground state character. It is well established that dissociation takes place on the ground electronic surface (152–157, 179–181, 207).

Above D_0, the excited resonances usually overlap, since the condition $\langle\Gamma\rangle\rho = N^\dagger/2\pi$, where $N^\dagger$ is the number of open channels in the TS, is usually obeyed. Note that ρ refers to the reactive density of states, which changes from a rovibronic to vibronic density with increasing energy as the decomposition time scale becomes shorter than characteristic time scales for IVR (203, 205, 208). Although previous studies of the decay rates and product state distributions have shown that, on the average, the decomposition of NO is well described by statistical theories (152–157, 179–181), in this review we focus on specific studies that probe fluctuations and effects due to overlapping resonances. First, we examine the relationship between spectral features in partial and total spectra and identify applicable conditions for the random phase approximation. We then examine the relationship between decay widths and the widths of features in these spectra, and probe the influence of thermal (initial state) averaging. Finally, we discuss the product state distributions and their implications for the dissociation mechanism and the TS.

The Relationship Between Partial and Total Absorption Spectra in the Regime of Overlapping Resonances

The experimental PHOFRY spectra show that when monitoring different final states, the spectral features differ in positions, line widths, and intensities (62–67). We use a simplified model to describe these observations that is based on assumptions inherent in statistical theories: (*a*) the parent eigenstates are ergodic and (*b*) formation and decay of the activated complex have uncorrelated phases (64, 65a,b, 209, 210). For a given set of resonances, the probability $[P_f(E)]$ of producing a final state f at energy E is given by the general form (64, 65a,b, 210)

$$P_f(E) = \left| \sum_m R_m(E) \cdot C_{fm} e^{i\phi_{fm}} \right|^2 = \left| \sum_m \frac{a_m \cdot C_{fm} e^{i\phi_{fm}}}{(E - E_m) + (i\Gamma_m/2)} \right|^2, \qquad 3.$$

where the amplitudes C_{fm} and phases ϕ_{fm} defining the projection of the resonance m on the final state f are real numbers taken as uniform random deviates in the intervals 0–1 and $0–2\pi$, respectively, and the amplitude of each resonance, $R_m(E)$, is given by (10a,b, 64, 65a,b, 210)

$$R_m(E) = \frac{a_m}{(E - E_m) + (i\Gamma_m/2)}. \qquad 4.$$

In Equation 4, E_m is the resonance energy, and a_m is the resonance excitation coefficient, which is proportional to Γ_m, the resonance width. In the case

of isolated resonances, Γ_m is directly related to the lifetime; however, when the resonances overlap, Γ_m cannot be observed, and the relationship between $\langle\Gamma(E)\rangle$ and $k(E)$ is not simple (209–211).

The expression given in Equation 3 has been obtained recently by using a random matrix version of Feshbach's optical model, where the coupling of the TS to the molecular complex is modeled via a universal random matrix effective Hamiltonian. This Hamiltonian is characterized by its resonance eigenstates and provides the correct average unimolecular decay rate in both loose [i.e. fragment-like (13a, 26a,b)] and tight TS cases (209, 210). The simplified description of Equation 3 yields calculated spectra qualitatively similar to ones obtained by the more rigorous treatment found in References 209 and 210. In analogy with the case of isolated resonances, the simplified model assumes that the coupling matrix elements to the continuum of fragment channels are random and that this in turn leads to randomly fluctuating decay widths obeying a chi-square-like distribution with n degrees of freedom. Here n is the number of states independently coupled to the zeroth-order levels (13a, 212–214); for loose and tight TSs n equals the number of open fragment channels and the number of energetically accessible states of the TS, respectively. In the calculations of Peskin et al (209, 210), as well as here, the excitation coefficients a_m are chosen as uniform random deviates, and the nearest neighbor level spacings of the resonances obey a Wigner-like distribution. We assume a chi-square distribution of decay widths (64, 65a,b) despite the fact that the distribution progressively deviates from this form as the degree of resonance overlap increases (210). We find that for a fixed $\langle\Gamma\rangle$, the simulations are not sensitive to the exact form of the width distribution (64, 65a,b, 210).

We compare in a qualitative way simulated spectra to experimental PHOFRY spectra obtained at $E^\dagger = 2000$–2525 cm^{-1}, where the degree of resonance overlap is substantial ($\langle\Gamma\rangle\rho > 5$) (64, 65a,b). We have recorded PHOFRY spectra in this region for 15 different NO final states (64, 65a,b), some of which are shown in Figure 3. The effects of interference are easily seen in the marked final state dependence of the widths, positions, and shapes of spectral features. Although not all populated NO product channels have been monitored, qualitative conclusions about the total absorption spectrum can be inferred from the sum of these 15 spectra, shown in Figure 6. Relative to the partial spectra, the summed spectrum clearly exhibits (*a*) an increase in background, (*b*) broader peaks, and (*c*) a decrease in the range of widths. Based on the reactive density of states, approximately 250 vibronic resonances lie in this region (201–206, 215); however, fewer than 20 peaks are observed in either partial or summed spectra. Consider also that the summed spectrum displays residual structure despite the summing of seemingly rather different spectra, which indicates that

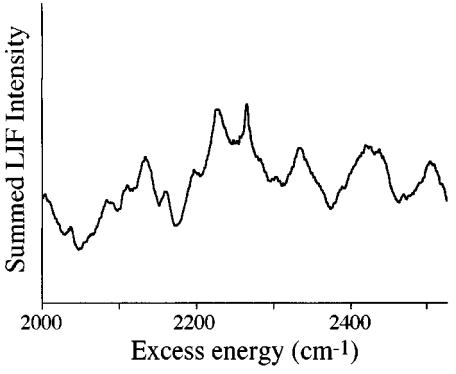

Figure 6 NO_2 IR-visible yield spectrum obtained by summing 15 individual PHOFRY spectra of NO($v = 0, 1$; J) obtained at $E^{\dagger} = 2000$–2500 cm^{-1}.

the partial spectra are correlated. This is not surprising when one recognizes that these spectra inherently arise from the same manifold of resonances.

Our simulated PHOFRY spectra are generated by using Equation 3 with a preselected random set of resonances, whose number reflects a vibronic density of states. Resonance widths are assigned about $\langle\Gamma\rangle$ from a chi-square-like distribution with n degrees of freedom, where n is the number of energetically accessible TS levels or independent decay channels. In the regime of overlapping resonances the decay rate $k(E)$ is not related to $\langle\Gamma\rangle$ in a simple manner (209); therefore, $\langle\Gamma\rangle$, ρ, and n are treated as independent parameters either taken from calculations (207, 216) or chosen to fit experimental data (62–67, 205). To qualitatively simulate the spectra shown in Figure 3, we use $n = 20$, $\langle\Gamma\rangle = 25$, and $\rho = 0.5$. The simulations are less sensitive to n and ρ and more sensitive to $\langle\Gamma\rangle$.

Given a set of resonances and an array of random coefficients C_{fm} and ϕ_{fm}, Equation 3 is used to generate a synthetic PHOFRY spectrum for a single fully quantum state–resolved decay channel. In order to properly account for the oxygen spin-orbit states and multiple parent rotational states, nine of these spectra are used to simulate PHOFRY spectra for individual NO quantum states (64, 65a,b). Several representative synthetic spectra are shown in the two upper panels of Figure 7, and the sum of 15 such spectra is shown as the solid line in the bottom panel. Note the qualitative similarities between the simulated and experimental spectra in terms of the number of peaks, range of widths, and differences among individual spectra.

It is instructive at this point to compare the simulated (summed) spectrum of Figure 7 to the spectrum obtained by incoherent superposition of the underlying

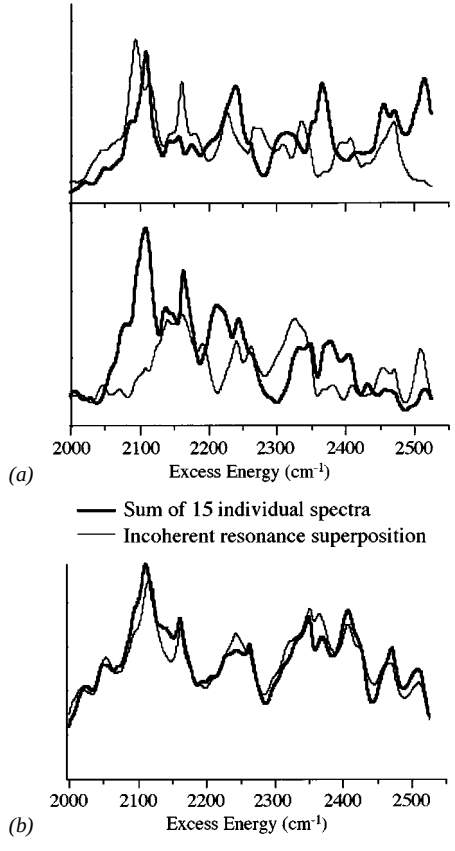

Figure 7 (*a*) Representative simulated spectra corresponding qualitatively to IR-visible PHOFRY spectra of NO_2 at $E^{\dagger} = 2000$–$2500\ cm^{-1}$. The parameters used in these simulations, $n = 20$, $\langle \Gamma \rangle = 25\ cm^{-1}$, and $\rho = 1/cm^{-1}$, were best chosen to simulate the experimental PHOFRY spectra. The level of incoherent averaging included in the calculated spectra roughly corresponds to that involved in the experimental IR-visible spectra when monitoring a single NO quantum state. (*b*) (*Thick line*) Sum of 15 individual simulated spectra such as those shown in panel *a*. (*Thin line*) Spectrum obtained by incoherent superposition of the resonances used in calculating the simulated spectra (Equation 5).

250 resonances in this spectral region, i.e.

$$I(E) = \sum_m |R_m(E)|^2 = \sum_m \frac{a_m^2}{(E - E_m)^2 + (\Gamma_m/2)^2}. \quad 5.$$

The spectrum generated by the single sum given by Equation 5 is shown as the dotted line in Figure 7. The two spectra are quite similar, indicating that the summation of 15 individual spectra is sufficient to average out most of the effects of phase and interference. Thus, although minor differences between the coherent and incoherent superpositions still exist, the random phase approximation is rather justified at this level of averaging. Using Equation 3, we have successfully simulated the experimental PHOFRY spectra in other regions of excess energy, as will be described in the following section (64, 65a,b, 210). In most cases, when a large number of spectra are summed, the spectra obtained by incoherent superposition of the underlying resonances are reproduced quite well.

In summary, both the experimental PHOFRY spectra and the simulated spectra clearly show the effects of interference due to overlapping resonances, which are manifested as marked changes in line shapes, positions, and widths among spectra obtained for different NO quantum states. The summation of a sufficiently large number of spectra obtained by monitoring different final states yields a spectrum similar to that obtained by incoherent superposition of all the underlying resonances; thus the random phase approximation is usually justified when dealing with averaged spectra. However, we note that when the number of final channels is small (e.g. near D_0 in NO_2) this approximation may not be justified (see below).

Widths of Spectral Features in the Regime of Overlapping Resonances

In the NO_2 PHOFRY spectra taken at $E^\dagger = 2000$–2525 cm^{-1}, it is clear by inspection that the resonances are overlapped. However, as a result of (*a*) the non-Lorentzian line shapes, (*b*) the marked final state dependence of the resonance line widths, and (*c*) the small number of observed peaks, a meaningful comparison between line widths and decay rates cannot be made. To examine this issue, we use simulated spectra of a region closer to threshold, where real-time measurements of $k(E)$ for jet-cooled samples are available (155–157). We note that in this region fewer channels are open and the degree of overlap, $\langle\Gamma\rangle\rho$, is necessarily smaller. We have previously shown that our model can qualitatively simulate state-selected PHOFRY spectra even just at D_0, where despite a small degree of overlap ($\langle\Gamma\rangle\rho \sim 0.64$) interference effects are still manifest. To understand this, we recognize that near D_0 the number of open channels n is smallest, and thus the decay width distribution is broadest. Although the degree of overlap is smaller on the average near D_0 than at higher

energies, overlaps will still arise owing to fluctuations in the decay widths for individual resonances.

Figure 8*a* displays two simulated spectra that correspond qualitatively to PHOFRY spectra in the region $E^{\dagger} = 100$–300 cm^{-1}. The parameters used in these simulations (chosen based on measured and/or calculated values) are $n = 8$, $\rho = 1/\text{cm}^{-1}$, and $\langle\Gamma\rangle = 3$ cm^{-1}. The individual spectra exhibit some differences, yet the sum of 15 such spectra still displays many sharp spectral features, as shown in Figure 8*b*. Note that for this lower degree of overlap, the summation of the individual spectra and the incoherent superposition of the 225 underlying resonances are similar, i.e. each shows ~ 30 peaks, many of which appear rather narrow. We have extracted widths for these features by treating them as single Lorentzians. The average width of the individual spectral features is 1.8 ± 0.1 cm^{-1} in the state-selected spectra and 2.6 cm^{-1} in the summed spectrum—a substantial broadening. The average widths of features in the state-specific spectra are thus narrower than the input average width (3 cm^{-1}), reflecting both the effects of interference and a bias in favor of narrow peaks when selecting peaks that appear isolated.

We note that the average width determined from the summed spectrum in Figure 8*b* is also smaller than, but closer to, the input average width. In this case, the number of summed channels (i.e. 15a,b) is sufficient to justify the random phase approximation. However, as the number of summed channels decreases (e.g. at energies closer to D_0), this approximation becomes less valid and the total absorption spectrum may retain features of the partial spectra (64, 65a,b, 209, 210). Of course, the degree of overlap is also smaller on the average near D_0, yet even here the PHOFRY spectra of NO_2 display the hallmarks of interference that are so obvious at higher energies (64, 65a,b, 67). Thus, when the number of open channels is small, the validity of extracting decay rates from widths in even total absorption spectra is questionable. We note that when resonances overlap, the average width cannot be linearly related to the average rate, but in fact the calculated rate is always smaller than that inferred from the average width (209). Thus, in the regime of overlapping resonances coupled to the same continuum, extracting average unimolecular decay rates from the widths of spectral features in final state–selected spectra is unjustified, even when many features appear sharp and isolated.

Effects of Thermal Averaging: One-Photon PHOFRY Spectra

The simulated and experimental PHOFRY spectra shown above demonstrate that the degree of overlap is important in determining the magnitude of interferences in the spectra obtained for different final states and that interference

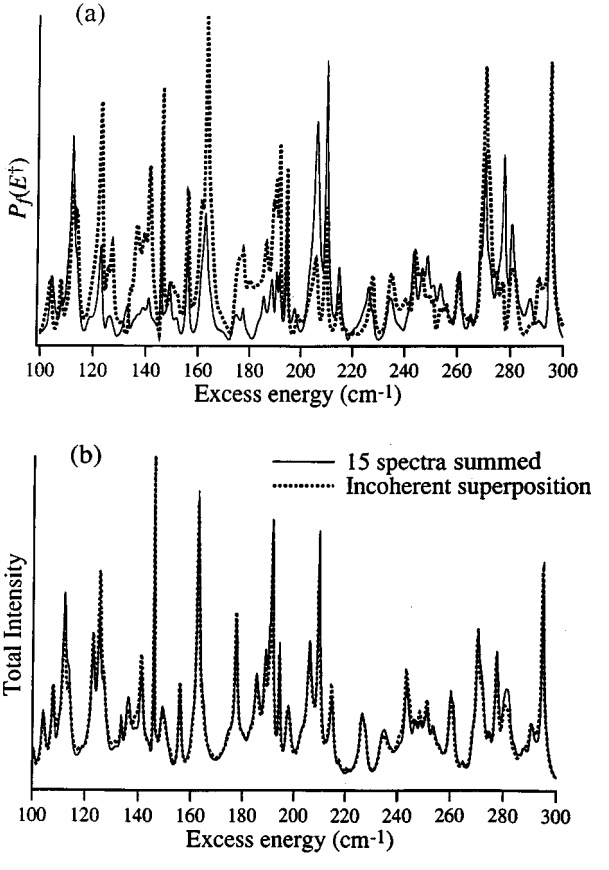

Figure 8 (*a*) Representative simulated spectra corresponding qualitatively to IR-visible PHOFRY spectra of NO_2 at $E^\dagger = 100$–300 cm^{-1}. The parameters used in these simulations are $n = 8$, $\langle\Gamma\rangle = 3$ cm^{-1}, and $\rho = 1/cm^{-1}$. (*b*) (*Thick line*) Sum of 15 individual simulated spectra such as those shown in panel *a.* (*Thin line*) Spectrum obtained by incoherent superposition of the resonances used in calculating the simulated spectra (Equation 5).

effects are rapidly washed out when summing over even a modest number of final states. We also expect incoherent superpositions resulting from initial state averaging to dampen, or even completely wash out, these effects. To investigate this, we compare one-photon and double-resonance IR-visible PHOFRY spectra obtained under identical conditions. A direct comparison of IR-visible and one-photon PHOFRY spectra is not possible because of differences in selection rules for the two excitation schemes (64); we therefore base our comparison on correlations within each set of spectra. The main difference between the two experiments is that the number of initial parent rotational levels accessed is significantly reduced in the state-selected experiment (64).

Figures 9*a* and 9*b* display pairs of one-photon PHOFRY spectra at $E^{\dagger} =$ 2150–2450 cm^{-1} obtained for NO levels of similar *J*. The spectra in each pair exhibit almost perfect correlation of the spectral features. Note, however, that different features are observed when comparing the different pairs of spectra, and thus levels of very different *J*. This illustrates the pronounced correlation between levels of similar *J* observed in the one-photon PHOFRY spectra obtained in this energy region (63). This correlation is not seen in the IR-visible spectra of this region (64, 65a,b), nor in fact do any pairs of IR-visible spectra display the level of correlation observed in Figure 9*a*. We have previously developed a quantitative measure of correlation, the correlation index, and the indices for these spectra support this conclusion (63–65a,b).

A second major difference between IR-visible and one-photon PHOFRY spectra is found in the resonance widths. The IR-visible PHOFRY spectra obtained at $E^{\dagger} =$ 2000–2500 cm^{-1} routinely display both narrower peaks and a larger number of peaks discernible from the background than the one-photon spectra. At these energies the average decay width ($\sim$ 15–20 cm^{-1}) (152–154, 207, 217) is significantly larger than the rotational envelope of a vibronic band ($\sim$ 5 cm^{-1}) at the characteristic rotational temperature of our experiment, $\sim$ 5 K (30). Excitation from different parent rotational levels thus primarily accesses the same set of overlapped vibronic levels, with relative excitation probabilities determined by line strength factors. Excitation from each parent rotational level coherently accesses these levels, and interferences produce specific spectral structures; however, the weightings of the resonances may be slightly different for different initial states, resulting in somewhat different spectra. Since excitation from different parent rotational levels is incoherent, the observed spectrum will be an incoherent superposition, displaying broader structures, as found above when comparing single-channel spectra versus spectra (incoherently) summed over many channels. This can explain why more narrow features are observed in IR-visible spectra and why these spectra lack correlations. We note that a similar type of broadening is exhibited when

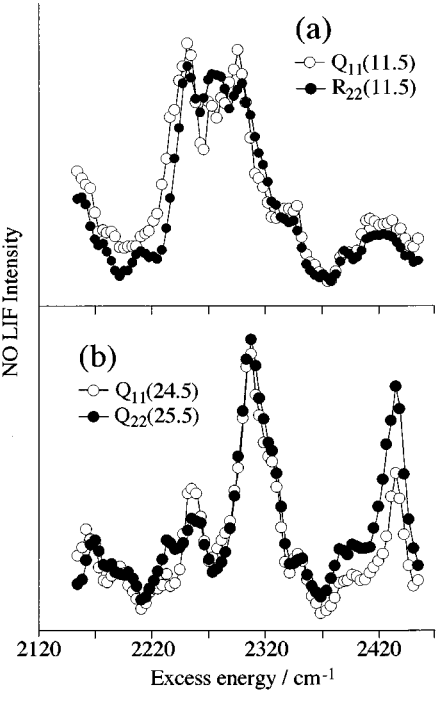

Figure 9 Representative NO_2 one-photon PHOFRY spectra at an excess energy $E^{\dagger} = 2100$–2450 cm^{-1}, obtained in each panel by monitoring NO($v = 0$) levels of similar J. Note the similarity of the two spectra in both (*a*) and (*b*), but the marked change in peak intensities, shapes, and widths of spectra in (*a*) vs (*b*).

PHOFRY spectra obtained by monitoring $O(^3P_j)$ states are compared to those of $NO(^2\Pi_\Omega, v, J, \Lambda)$ states. Each $O(^3P_j)$ spectrum is in fact a superposition of many spectra correlated with the open NO channels, and thus exhibits much broader spectral features (166, 168).

Product State Distributions: The Importance of the PES

The case of HCO is an example of the triumph of quantum dynamical calculations carried out on multidimensional ab initio PESs in describing the observed trends in nascent fragment state distributions, even at a state-to-state level of detail. Calculations of this detail are currently not available for NO_2, and our approach has been to compare the PSDs with predictions of statistical models, which require knowledge of the PES only in the TS region. We note that for other small molecules whose unimolecular decompositions have been studied

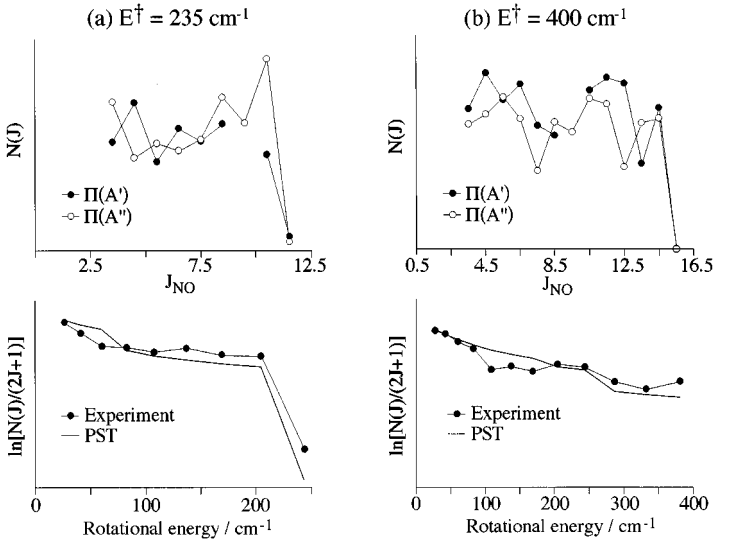

Figure 10 NO($^2\Pi_{1/2}$,$v = 0$) rotational state distributions from NO_2 decomposition following IR-visible excitation at excess energies of (*a*) $E^\dagger = 235\ cm^{-1}$ and (*b*) $E^\dagger = 400\ cm^{-1}$. The top plot in each panel displays the individual Λ-doublet distributions, while the bottom Boltzmann-type plot shows the distribution summed over Λ-doublet level compared with the prediction of phase space theory (PST).

state-selectively [e.g. NCNO (22–27) and CH_2CO (13a,b, 42–49)] remarkable agreement has been found with the predictions of statistical theories. Detailed descriptions of these theories are found elsewhere (13a, 26a,b, 218–230) and will not be elaborated upon here.

Figures 10 and 11 display selected NO($v = 0$) rotational distributions at energies near and significantly above D_0, respectively, obtained from decomposition of jet-cooled NO_2 following both IR-visible and one-photon excitation. As illustrated in Figure 10, the individual Λ-doublet distributions of the NO fragment obtained at energies near D_0 exhibit essentially random fluctuations, a trend observed by other workers as well (66a,b, 67, 159). However, these fluctuations consistently scatter around the theoretical predictions of phase space theory (PST). The distributions summed over Λ-doublet level show reduced fluctuations and good agreement with PST, even for IR-visible excitation.

The NO($v = 0$) rotational distributions shown in Figure 11, which are representative for excess energies significantly above D_0 (e.g. $E^\dagger > 2000\ cm^{-1}$), display pronounced oscillatory structures that are well reproduced in the two Λ-doublet level distributions [as well as the two NO spin-orbit states (63–65b)]

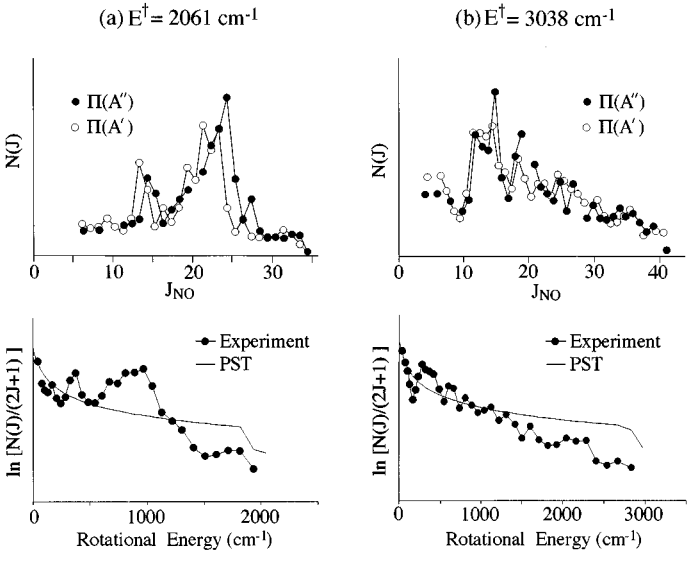

Figure 11 NO($^2\Pi_{1/2}$,$v = 0$) rotational state distributions from NO_2 decomposition following one-photon excitation at excess energies of (*a*) $E^\dagger = 2061\ cm^{-1}$ and (*b*) $E^\dagger = 3038\ cm^{-1}$. The top plot in each panel displays the individual Λ-doublet distributions, while the bottom Boltzmann-type plot shows the distribution summed over Λ-doublet level compared with the prediction of PST.

and are not diminished when summing over Λ-doublet level. We have previously shown that these oscillations can be modeled qualitatively by mapping bending-like wave functions associated with a tight TS into free rotor states of the NO fragment (64, 65a,b). Thus, the change in fluctuation patterns reveals the progressive tightening of the TS (13a, 64, 65a,b, 135). It is therefore intriguing to note that the oscillations consistently cluster about the statistical predictions of PST, which assumes a very loose TS. This apparent discrepancy can be reconciled by recognizing that the range of rotational excitation allowed in this mapping is a sensitive function of the TS bending angle and frequency. The TS parameters used were based on values derived from ab initio calculations (173, 207) and happen to correspond to rotational excitations that cover the full range allowed by energy conservation up to the highest energies studied ($E^\dagger \sim 3000$ cm^{-1}). The qualitative agreement observed with PST at these energies thus reflects in part the specific geometry of the tight TS and does not constitute a valid test for the location of the TS. This underscores the importance of the PES and illustrates an important point: Distributions that can be fit by a statistical model do not prove that such a model correctly describes the dissociation mechanism. We note that the observation of PST-like distributions in this case may also arise

from exit-channel interactions beyond the TS, which can lead to population of all levels allowed by energy and angular momentum conservation.

The relative vibrational populations of the NO fragment were measured by us at a number of excess energies from the energetic threshold of NO($v = 1$) at $E^\dagger = 1876$ cm^{-1} to 3038 cm^{-1} (179, 180). Good qualitative agreement with the predictions of variational RRKM theory is observed, although the experimental values tend to fluctuate about the statistical predictions (65a,b, 180, 207). In contrast, the NO($^2\Pi_\Omega$; $\Omega = 1/2$, 3/2) spin-orbit state distributions over the same range are colder than expected by statistical models, in both the $v = 0$ and $v = 1$ channels (179–181). Similarly, spin-orbit state distributions that are colder than statistical are found for the O(^3P_j; $j = 2$, 1, 0) fragment (166, 168). While the relative O(^3P_j) populations show marked fluctuations with excess energy (166, 168), the overall ratio NO($^2\Pi_{1/2}$; $v = 0$, 1)/NO($^2\Pi_{3/2}$; $v = 0$, 1) ~ 3 varies only slightly with photolysis energy over this range (180). These trends can be understood in light of the recent work of Katagiri & Kato (173), who calculated ab initio all 18 doubly degenerate O-NO PESs correlated with the various NO($^2\Pi_\Omega$) + O(^3P_j) asymptotes. Using these potentials and a simplified model of the dissociation, average spin-orbit state distributions of both fragments were calculated, in good agreement with experiment. We note that these calculations also predict the trends in correlated NO($^2\Pi_\Omega$) + O(^3P_j) distributions (181).

A critical examination of the NO PSDs underscores the need for ab initio PESs in understanding trends in fragment state distributions, since PSDs can often be modified via exit-channel interactions beyond the TS. For molecules with distinct exit-channel barriers (e.g. HFCO, HCO), dynamical signatures in the PSDs are usually prominent. In the absence of such barriers, the exit-channel gradients are typically small and recoil velocities are low, especially for products whose internal energies approach $E^\dagger$. As a consequence, the dynamics in this case is rarely dominated by simple propensity rules. Energy exchange beyond the TS needs to be better understood and is probably governed by a subtle interplay between the size of the energy quantum to be transferred and the relative recoil velocity.

CONCLUDING REMARKS

In recent years, we have witnessed tremendous progress in our understanding of unimolecular reactions on a fully state-resolved level. Such progress is due in large part to experimental advances that allow the preparation of reactants in single quantum states and detailed measurements of observables, including dissociation rates and correlated product quantum state distributions. These advances have led to stringent tests of the connection between resonant scattering

and statistical behavior and afforded rigorous tests of the central assumptions of statistical theories. For small molecules with low threshold energies for reaction, IVR is usually incomplete and striking mode and state specificity is often observed. This specificity can only be understood with detailed knowledge of the full PES. In contrast, for larger systems where IVR is essentially complete, marked fluctuations may be observed for specific resonances, but agreement on the average with the predictions of statistical models is expected. The competition between IVR and decomposition rate is central to our ability to implement bond- and mode-selective chemistry and will continue to be explored.

When resonances overlap, interference effects may become prominent. It is important to ask how general this phenomenon is, since such effects have been identified experimentally only for NO_2 (62–67) and H_2CO (13b). We have seen that fluctuations arise even in the isolated regime; therefore, overlapping resonances are implicated only when the partial spectra show variations in shapes, widths, and intensities of the observed features as a function of the monitored fragment state, or in other cases where strongly asymmetric line shapes are observed (13b). We believe that fluctuations and oscillations due to overlapping resonances will be observed in the unimolecular reactions of other small molecules when one of the products is an atom and the initial state is well defined.

Despite recent progress, there are clearly areas that require further investigation. Examples include the role of parent rotation and centrifugal barriers [e.g. measurements of $k(E, J)$], the importance of long-range forces and energy transfer via exit-channel interactions, the issue of adiabaticity for different degrees of freedom, the conservation of specific quantum numbers in the dissociation, the manifestations of restricted IVR and its dependence on $E^{\dagger}$, and the transition from statistics to dynamics at high $E^{\dagger}$. Many sophisticated experimental techniques are now available to explore these issues at ever increasing levels of detail, and intense theoretical effort is directed both towards multidimensional ab initio calculations of PESs and dynamical methods for treating resonances and their evolution. The interplay between experiment and theory is crucial and rewarding and will lead to a deeper and comprehensive understanding of these processes.

ACKNOWLEDGMENTS

We would like to thank C Wittig, HS Taylor, R Schinke, J Troe, CB Moore, WH Miller, U Peskin, and A Sanov for many enlightening discussions. We thank R Schinke, E A Rohlfing, PL Houston, and F Temps for sending us reprints and preprints of their work. HR gratefully acknowledges support by the National Science Foundation, the Department of Energy, and the Army Research Office.

Literature Cited

1. Blatt JM, Wiesskopf VF. 1979. *Theoretical Nuclear Physics.* New York: Springer
2. Feshbach H. 1992. *Theoretical Nuclear Physics: Nuclear Reactions.* New York: Wiley
3. Truhlar DG, ed. 1984. *Resonances in Electron-Molecule Scattering, van der Waals Complexes, and Reactive Chemical Dynamics.* Washington DC: Am. Chem. Soc.

4a. Hinze J, ed. 1980. *Electron-Atom and Electron-Molecule Collisions.* New York: Plenum
4b. Massey HSW, Burhop EHS, Gilbody HB. 1969. *Electronic and Ionic Impact Phenomena.* London: Oxford Univ.
4c. Burke PG. 1989. In *Collision Theory for Atoms and Molecules*, ed. FA Gianturco, pp. 11–58. New York: Plenum
4d. Domcke W. 1991. *Phys. Rep.* 208:97–122

5. Lawley KP, ed. 1985. *Photodissociation and Photoionization.* New York: Wiley
6. Schinke R. 1993. *Photodissociation Dynamics.* Cambridge: Cambridge Univ.
7. Beswick JA, Jortner J. 1981. *Adv. Chem. Phys.* 47:363

8a. Child MS. 1974. *Molecular Collision Theory.* London: Academic
8b. Bosanac SD. 1988. *Long-Lived States in Collisions.* Boca Raton: CRC

9. Satchler G. 1990. *Introduction to Nuclear Reactions.* New York: Oxford Univ.

10a. Ericson T. 1963. *Ann. Phys.* 23:390–414
10b. Ericson T. 1960. *Phys. Rev. Lett.* 5:430–31

11. Mies FH, Krauss M. 1966. *J. Chem. Phys.* 45:4455–68

12a. Schinke R, Keller H-M, Stumpf M, Dobbyn AJ. 1995. *J. Phys. B: At. Mol. Opt. Phys.* 28:3081–111
12b. Reisler H, Keller H-M, Schinke R. 1994. *Comments At. Mol. Phys.* 30:191–220
12c. Schinke R, Keller H-M, Stumpf M, Dobbyn AJ. 1996. *Faraday Discuss. Chem. Soc.* 102:In press

13a. Green WH Jr, Moore CB, Polik WF. 1992. *Annu. Rev. Phys. Chem.* 43:591–626
13b. Polik WF, Moore CB, Miller WH. 1988. *J. Chem. Phys.* 89:3584–91

14. Bamford DJ, Filseth SV, Foltz MF, Hepburn JW, Moore CB. 1985. *J. Chem. Phys.* 82:3032–41

15a. Miller WH, Hernandez R, Moore CB, Polik WF. 1990. *J. Chem. Phys.* 93: 5657–66
15b. Hernandez R, Miller WH, Moore CB, Polik WF. 1993. *J. Chem. Phys.* 99:950–62

16. Polik WF, Guyer DR, Moore CB. 1990. *J. Chem. Phys.* 92:3453–70

17a. Polik WF, Guyer DR, Miller WH, Moore CB. 1990. *J. Chem. Phys.* 92:3471–84
17b. Guyer DR, Polik WF, Moore CB. 1986. *J. Chem. Phys.* 84:6519–21

18. Butenhoff TJ, Carleton K, Moore CB. 1990. *J. Chem. Phys.* 92:377–93
19. Carleton K, Butenhoff TJ, Moore CB. 1990. *J. Chem. Phys.* 93:3907–18
20. Butenhoff TJ, Carleton K, Chuang M-C, Moore CB. 1989. *J. Chem. Soc. Faraday Trans. 2* 85:1155–67
21. van Zee RD, Foltz MF, Moore CB. 1993. *J. Chem. Phys.* 99:1664–73
22. Nadler I, Noble M, Reisler H, Wittig C. 1985. *J. Chem. Phys.* 82:2608–19
23. Qian CXW, Noble M, Nadler I, Reisler H, Wittig C. 1985. *J. Chem. Phys.* 83:5573–80
24. Wittig C, Nadler I, Reisler H, Noble M Catanzarite J, Radhakrishnan G. 1985. *J. Chem. Phys.* 83:5581–88
25. Qian CXW, Ogai A, Reisler H, Wittig C. 1989. *J. Chem. Phys.* 90:209–18

26a. Reisler H, Wittig C. 1986. *Annu. Rev. Phys. Chem.* 37:307–49
26b. Reisler H, Wittig C. 1992. In *Advances in Kinetics and Dynamics*, ed. JR Barker. 1:139–86. Greenwich: JAI Press

27. Klippenstein SJ, Khundkar LR, Zewail AH, Marcus RA. 1988. *J. Chem. Phys.* 89:4761–70
28. Rizzo TR, Hayden CC, Crim FF. 1984. *J. Chem. Phys.* 81:4501–9
29. Rizzo TR, Hayden CC, Crim FF. 1983. *Faraday Discuss. Chem. Soc.* 75:276–77

30. Crim FF. 1984. *Annu. Rev. Phys. Chem.* 35:657–91
31. Dübal HR, Crim FF. 1985. *J. Chem. Phys.* 83:3863–72
32. Ticich TM, Rizzo TR, Dübal HR, Crim FF. 1986. *J. Chem. Phys.* 84:1508–20
33. Brouwer L, Cobos CJ, Troe J, Dübal HR, Crim FF. 1987. *J. Chem. Phys.* 86:6171–82
34. Butler LJ, Ticich TM, Likar MD, Crim FF. 1986. *J. Chem. Phys.* 85:2331–32
35. Scherer NF, Zewail AH. 1987. *J. Chem. Phys.* 87:97–114
36. Luo X, Rizzo T. 1990. *J. Chem. Phys.* 93:8620–33
37. Luo X, Fleming PR, Seckal TA, Rizzo TR. 1990. *J. Chem. Phys.* 93:9194–96
38. Foy BR, Casassa MP, Stephenson JC, King DS. 1988. *J. Chem. Phys.* 89:608–9
39. Foy BR, Casassa MP, Stephenson JC, King DS. 1989. *J. Chem. Phys.* 90:7037–45
40. Alexander MH, Werner H-J, Dagdigian P. 1988. *J. Chem. Phys.* 89:1388–400
41. Alexander MH, Werner H-H, Hemmer T, Knowles PJ. 1990. *J. Chem. Phys.* 93:3307–18
42. Chen I-C, Green WH Jr, Moore CB. 1988. *J. Chem. Phys.* 89:314–28
43. Chen I-C, Moore CB. 1988. *J. Phys. Chem.* 94:263–68
44. Chen I-C, Moore CB. 1988. *J. Phys. Chem.* 89:269–74
45. Green WH Jr, Chen I-C, Moore CB. 1988. *Ber. Bunsenges. Phys. Chem.* 84:389–96
46. Green WH Jr, Mahoney AJ, Zheng Q-K, Moore CB. 1991. *J. Chem. Phys.* 94:1961–69
47a. Garcia-Moreno I, Lovejoy ER, Moore CB. 1994. *J. Chem. Phys.* 100:8890–901
47b. Garcia-Moreno I, Lovejoy ER, Moore CB. 1994. *J. Chem. Phys.* 100:8902–6
48. Potter ED, Gruebele M, Khundkar LR, Zewail AH. 1989. *Chem. Phys. Lett.* 164:463–70
49. Kim S-K, Choi YS, Pibel CD, Zheng Q-K, Moore CB. 1991. *J. Chem. Phys.* 94:1954–60
50. Mies FH. 1968. *Phys. Rev.* 175:164–75
51. Hase WL, Cho S-W, Lu D-H, Swamy KN. 1989. *Chem. Phys.* 139:1–13
52. Hartke B, Manz J, Mathis J. 1989. *Chem. Phys.* 139:123–46
53. Noble M, Qian CXW, Reisler H, Wittig C. 1986. *J. Chem. Phys.* 85:5763–73
54. Fano U. 1961. *Phys. Rev.* 124:1866
55. Brandon JT, Reid SA, Robie DC, Reisler H. 1992. *J. Chem. Phys.* 97:5246–49
56. Reid SA, Brandon JT, Reisler H. 1993. *J. Phys. Chem.* 97: 540–43
57. Brandon JT. 1995. *State-specific photodissociation of small polyatomic molecules: nitrosyl fluoride and methyl nitrite*. PhD thesis. Univ. Southern Calif.
58a. Suter HU, Huber JR, von Dirke M, Untch A, Schinke R. 1992. *J. Chem. Phys.* 96:6643–53
58b. Dobbyn AJ, von Dirke M, Schinke R, Fink R. 1995. *J. Chem. Phys.* 102:7070–79
59. Cotting R, Huber JR, Engel V. 1994. *J. Chem. Phys.* 100:1040–46
60. Shapiro M, Reisler H. 1995. *J. Chem. Phys.* 103:4150–56
61. Lefebvre-Brion H, Field RW. 1986. *Perturbations in the Spectra of Diatomic Molecules.* Orlando: Academic
62. Reid SA, Brandon JT, Hunter M, Reisler H. 1993. *J. Chem. Phys.* 99:4860–63
63. Reid SA, Robie D, Reisler H. 1994. *J. Chem. Phys.* 100:4256–71
64. Reid SA, Reisler H. 1994. *J. Chem. Phys.* 101:5683–99
65a. Reid SA, Reisler H. 1996. *J. Phys. Chem.* 100:474–87
65b. Reid SA, Sanov A, Reisler H. 1996. *Faraday Discuss. Chem. Soc.* 102:In press
66a. Robra U, Zacharias H, Welge KH. 1990. *Z. Phys. D* 16:175–88
66b. Robra U. 1984. PhD thesis, Univ. Bielefeld
67. Miyawaki J, Yamanouchi K, Tsuchiya S. 1993. *J. Chem. Phys.* 99:254–64
68. Miecher E, Huber KP. 1976. *International Review of Science, Physical Chemistry, Series 2*. 3:37. London: Butterworths
69. Gobeli DA, Young JJ, El-Sayed MA. 1985. *Chem. Rev.* 85:529–54
70. Levy DH, Wharton L, Smalley RE. 1977. In *Chemical and Biochemical Applications of Lasers*, ed. CB Moore, 2:1–41. New York: Academic
71. Hamilton CE, Kinsey JL, Field RW. 1986. *Annu. Rev. Phys. Chem.* 37:493–524
72. Dai HL. 1991. In *Advances in Multiphoton Processes and Spectroscopy*, ed. SH Lin, Vol. 7. Singapore: World Sci.
73. Dai H-L, Field RW, eds. 1994. *Molecular Dynamics and Spectroscopy by Stimulated Emission Pumping.* Singapore: World Sci.
74. Dai H-L, ed. 1990. *J Opt. Soc. Am.* 7:1802–3
75. Ng C-Y, ed. 1994. *Advances in Physical Chemistry.* Singapore: World Sci.

76. Andresen P, Beushausen V, Häusler D, Lulf HW, Rothe EW. 1985. *J. Chem. Phys.* 83:1429–30
77. Schinke R, Engel V, Andresen P, Häusler D, Balint-Kurti GG. 1985. *Phys. Rev. Lett.* 55:1180–83
78. Zhang Q, Kandel SA, Wasserman TAW, Vaccaro PH. 1992. *J. Chem. Phys.* 96:1640–43
79. Buntine MA, Chandler DW, Hayden CC. 1992. *J. Chem. Phys.* 97:707–10
80. Butenhoff TJ, Rohlfing EA. 1992. *J. Chem. Phys.* 97:1595–98
81. Williams S, Tobiason JD, Dunlop JR, Rohlfing EA. 1995. *J. Chem. Phys.* 102:8342–58
82. Tobiason JD, Dunlop JR, Rohlfing EA. 1995. *J. Chem. Phys.* 103:1448–69
83. Abel B, Hamann HH, Lange N. 1996. *Faraday Discuss. Chem. Soc.* 102:In press
84. Abel B, Hamann HH, Lange N, Troe J. 1996. *J. Chem. Phys.* In press
85. Abrams RL, Lam JF, Lind RC, Steel DG, Liao PF. 1983. In *Optical Phase Conjugation*, ed. RA Fisher, pp. 211–84. New York: Academic
86. Hall G, Suits AG, Whitaker BJ. 1993. *Chem. Phys. Lett.* 203:277–82
87. Okazaki A, Ebata T, Mikami N. 1995. *Chem. Phys. Lett.* 241:275–80
88. Butenhoff TJ, Rohlfing EA. 1993. *J. Chem. Phys.* 98:5460–68
89. Butenhoff TJ, Rohlfing EA. 1993. *J. Chem. Phys.* 98:5469–76
90. Buntine MA, Chandler DW, Hayden CC. 1995. *J. Chem. Phys.* 102:2718–26
91. O'Keefe A, Deacon DAG. 1988. *Rev. Sci. Instrum.* 59:2544–51
92. Choi YS, Teal P, Moore CB. 1990. *J. Opt. Soc. Am. B* 7:1829–34
93. Dixon RN. 1986. *J. Chem. Phys.* 85:1866–79
94. Milligan DE, Jacox ME. 1964. *J. Chem. Phys.* 41:3032–36
95. Milligan DE, Jacox ME. 1969. *J. Chem. Phys.* 51:277–88
96. Ewing GE, Thompson WE, Pimentel GC. 1960. *J. Chem. Phys.* 32:927–32
97. Shirk JS, Pimentel GC. 1968. *J. Am. Chem. Soc.* 90:3349–51
98. Ogilvie JF. 1967. *Spectrochim. Acta A* 23:737–50
99. Brown JM, Ramsay DA. 1975. *Can. J. Phys.* 53:2232–41
100. Johns JWC, McKellar ARW, Riggin M. 1977. *J. Chem. Phys.* 67:2427–35
101. Brown JM, Buttenshaw J, Carrington A, Dumper K, Parent CR. 1980. *J. Mol. Spectrosc.* 79:47–61
102. Landsberg BM, Merer AJ, Oka T. 1977. *J. Mol. Spectrosc.* 67:459–75
103. Stone BM, Noble M, Lee EKC. 1985. *Chem. Phys. Lett.* 118:83–87
104. Murray KK, Miller TM, Leopold DG, Lineberger WC. 1986. *J. Chem. Phys.* 84:2520–25
105. Dane CB, Lander DR, Curl RF, Tittel FK, Guo Y, et al. 1988. *J. Chem. Phys.* 88:2121–28
106. Sappey AD, Crosley DR. 1990. *J. Chem. Phys.* 93:7601–8
107. Adamson GW, Zhao X, Field RW. 1993. *J. Mol. Spectrosc.* 160:11–38
108. Neyer DW, Luo X, Houston PL, Burak I. 1993. *J. Chem. Phys.* 98:5095–98
109. Neyer DW, Luo X, Houston PL, Burak I. 1995. *J. Chem. Phys.* 102:1645–57
110. Neyer DW, Houston PL. 1994. In *The Chemical Dynamics and Kinetics of Small Radicals*, ed. K Liu, A Wagner. Singapore: World Sci.
111. van Zee RD, Pibel CD, Butenhoff TJ, Moore CB. 1992. *J. Chem. Phys.* 97:3235–44
112. Burak I, Hepburn JW, Sivakumar N, Hall GE, Chawla G, Houston PL. 1987. *J. Chem. Phys.* 86:1258–68
113. Choi YS, Moore CB. 1995. *J. Chem. Phys.* 103:9981–88
114. Bowman JM, Bittman JS, Harding LB. 1986. *J. Chem. Phys.* 85:911–21
115. Romanowski H, Lee K-T, Bowman JM, Harding LB. 1986. *J. Chem. Phys.* 84:4888–93
116. Wagner AF, Bowman JM. 1987. *J. Phys. Chem.* 91:5314–24
117. Bowman JM, Gazdy B, Cho S-W, Wagner AF. 1991. *J. Chem. Phys.* 94:4192–94
118. Cho S-W, Wagner AF, Gazdy B, Bowman JM. 1992. *J. Chem. Phys.* 96:2799–811
119. Cho S-W, Wagner AF, Gazdy B, Bowman JM. 1992. *J. Chem. Phys.* 96:2812–18
120. Cho S-W, Wagner AF, Gazdy B, Bowman JM. 1991. *J. Phys. Chem.* 95:9897–901
121. Bowman JM, Gazdy B. 1991. *J. Chem. Phys.* 94:816–17
122. Bowman JM, Gazdy B. 1992. *Chem. Phys. Lett.* 200:311–17
123. Christoffel KM, Bittman JS, Bowman JM. 1987. *Chem. Phys. Lett.* 133:525–30
124. Wang D, Bowman JM. 1994. *J. Chem. Phys.* 100:1021–27
125. Wang D, Bowman JM. 1995. *Chem. Phys. Lett.* 235:277–85

126. Gray SK. 1992. *J. Chem. Phys.* 96:6543–54
127. Dixon RN. 1992. *J. Chem. Soc. Faraday Trans.* 88:2575–82
128. Werner H-J, Bauer C, Rosmus P, Keller H-M, Stumpf M, Schinke R. 1995. *J. Chem. Phys.* 102:3593–611
129. Keller H-M, Floethmann H, Stumpf M, Schinke R, Werner H-J, et al. 1996. *J. Chem. Phys.* In press
130. Tobiason JD, Dunlop JR, Rohlfing EA. 1995. *Chem. Phys. Lett.* 235:268–76
131. Temps F. 1995. Private communication
132. Schinke R. 1995. Private communication
133. Choi YS, Moore CB. 1989. *J. Chem. Phys.* 90:3875–76
134. Moore CB, Choi YS, Guyer DR, Polik WF, Zheng Q-K. 1990. In *Laser Spectroscopy IX*, ed. MS Feld, JE Thomas, A Mooradian. New York: Academic
135. Moore CB, Zheng Q-K, Choi YS, Green WH, Kim SK, et al. 1990. *Philos. Trans. R. Soc. London Ser. A* 332:297–307
136. Choi YS, Moore CB. 1991. *J. Chem. Phys.* 94:5414–25
137. Choi YS, Moore CB. 1992. *J. Chem. Phys.* 97:1010–21
138. Miller WH. 1983. *J. Am. Chem. Soc.* 105:216–20
139. Morokuma K, Kato S, Hirao K. 1980. *J. Chem. Phys.* 72:6800–2
140. Kamiya K, Morokuma K. 1991. *J. Chem. Phys.* 94:7287–98
141. Goddard JD, Schaefer HF III. 1990. *J. Chem. Phys.* 93:4907–15
142. Francisco JS, Zhao Y. 1992. *J. Chem. Phys.* 96:7587–96
143. Wei T-G, Wyatt RE. 1993. *J. Phys. Chem.* 97:13580–85
144. Miller WH, Handy NC, Adams J. 1980. *J. Chem. Phys.* 72:99–112
145a. Geers A, Kappert J, Temps F, Weibrecht JW. 1990. *J. Chem. Phys.* 93:1472–73
145b. Geers A, Kappert J, Temps F, Weibrecht JW. 1993. *J. Chem. Phys.* 98:4297–38
146. Geers A, Kappert J, Temps F, Weibrecht JW. 1993. *J. Chem. Phys.* 99:2271–79
147. Geers A, Kappert J, Temps F, Weibrecht JW. 1994. *J. Chem. Phys.* 101:3618–33
148. Geers A, Kappert J, Temps F, Weibrecht JW. 1994. *J. Chem. Phys.* 101:3634–48
149. Dertinger S, Geers A, Kappert J, Temps F, Wiebrecht JW. 1996. *Faraday Discuss. Chem. Soc.* 102:In press
150. Temps F. 1994. See Ref. 73
151. Chen CH, Clark DW, Payne MG, Kramer SD. 1980. *Opt. Commun.* 32:391–98
152. Gaedkte H, Hippler H, Troe J. 1972. *Chem. Phys. Lett.* 16:177–79
153. Gaedkte H, Troe J. 1975. *Ber. Bunsenges. Phys. Chem.* 79:184–91
154. Quack M, Troe J. 1975. *Ber. Bunsenges. Phys. Chem.* 79:469–79
155. Brucker GA, Ionov SI, Chen Y, Wittig C. 1992. *Chem. Phys. Lett.* 194:301–8
156. Ionov SI, Brucker GA, Jaques C, Chen Y, Wittig C. 1993. *J. Chem. Phys.* 99:3420–35
157. Ionov SI, Wittig C. 1994. *J. Chem. Phys.* 100:4714–15
158. Ionov SI, Bazel I, Wittig C. 1995. In *Femtochemistry: The Lausanne Conference*, ed. S Chrgui. Singapore: World Sci.
159. Zacharias H, Geilhaupt M, Meier K, Welge KH. 1981. *J. Chem. Phys.* 74: 218–25
160. Zacharias H, Meier K, Welge KH. 1983. In *Energy Storage and Redistribution in Molecules*, ed. J Hinze. New York: Plenum
161. Mons M, Dimicoli I. 1986. *Chem. Phys. Lett.* 131:298–302
162. Mons M, Dimicoli I. 1989. *Chem. Phys.* 130:307–24
163. Kawasaki, M, Sato H, Fukuroda A, Kikuchi T, Kobayashi S, Arikawa T. 1987. *J. Chem. Phys.* 86:4431–37
164. Chen K, Pei C. 1987. *Chem. Phys. Lett.* 137:361–64
165. Rubahn H-G, van der Zande WJ, Zhang R, Bronikowski MJ, Zare RN. 1991. *Chem. Phys. Lett.* 186:154–60
166. Miyawaki J, Tsuchizawa T, Yamanouchi K, Tsuchiya S. 1990. *Chem. Phys. Lett.* 165:168–70
167. Miyawaki J, Yamanouchi K, Tsuchiya S. 1994. *J. Chem. Phys.* 100:4716–17
168. Miyawaki J, Yamanouchi K, Tsuchiya S. 1991.*Chem. Phys. Lett.* 180:287–92
169. Elofson P-A, Ljungstrom E. 1992. *Chem. Phys.* 165:323–37
170. Changlong N, Hua L, Pfab J. 1993. *J. Phys. Chem.* 97:7458–64
171. Hradil VP, Suzuki T, Hewitt SA, Houston PL, Whitaker BJ. 1993. *J. Chem. Phys.* 99:4455–63
172. Rohlfing EA, Valentini JJ. 1985. *J. Chem. Phys.* 83:521–28
173. Katagiri H, Kato S. 1993. *J. Chem. Phys.* 99:8805–15
174. Busch GE, Wilson K. 1972. *J. Chem. Phys.* 56:3626–37
175. Busch GE, Wilson K. 1972. *J. Chem. Phys.* 56:3638–54
176. McFarlane J, Polanyi JC, Shapter JG. 1991. *J. Photochem. Photobiol. A* 58: 139–72

177. Harrison JA, Yang X, Rösslein M, Felder P, Huber JR. 1994. *J. Phys. Chem.* 98:12260–69
178. Knepp PT, Terentis AC, Kable SH. 1995. *J. Chem. Phys.* 103:194–204
179. Robie DC, Hunter M, Bates JL, Reisler H. 1992. *Chem. Phys. Lett.* 193:413–22
180. Hunter M, Reid SA, Robie DC, Reisler H. 1993. *J. Chem. Phys.* 99:1093–108
181. Sanov A, Bieler C, Reisler H. 1995. *J. Phys. Chem.* 99:7339–51
182. Douglas AE, Huber KP. 1965. *Can. J. Phys.* 43:74–81
183. Douglas AE. 1966. *J. Chem. Phys.* 45:1007–15
184. Hsu D, Monts DL, Zare RN. 1978. *Spectral Atlas of Nitrogen Dioxide 5530 to 6480 Å*. New York: Academic
185. Brucat PJ, Zare RN. 1985. *Mol. Phys.* 55:277–85
186. Köppel H, Domcke W, Cederbaum LS. 1984. *Adv. Chem. Phys.* 57:59–246
187. Haller E, Köppel H, Cederbaum LS. 1985. *J. Mol. Spectrosc.* 111:377–97
188. Zimmermann Th, Köppel H, Cederbaum LS. 1989. *J. Chem. Phys.* 91:3934–47
189. Zimmermann Th, Cederbaum LS, Meyer H-D, Köppel H. 1987. *J. Phys. Chem.* 91:4446–55
190a. Zimmermann Th, Cederbaum LS, Köppel H. 1988. *Ber. Bunsenges. Phys. Chem.* 92:217–21
190b. Manthe U, Meyer H-D, Cederbaum LS. 1992. *J. Chem. Phys.* 97:9062–71
191. Brand JCD, Chiu PH. 1977. *J. Mol. Spectrosc.* 75:1–9
192. Persch G, Vedder HJ, Demtröder W. 1986. *Chem. Phys.* 105:471–79
193. Persch G, Vedder HJ, Demtröder W. 1987. *J. Mol. Spectrosc.* 123:356–65
194. Vedder HJ, Schwarz M, Foth H-J, Demtröder W. 1983. *J. Mol. Spectrosc.* 97:92–116
195. Persch G, Mehdizadeh E, Demtröder W, Zimmermann Th, Köppel H, Cederbaum LS. 1988. *Ber. Bunsenges. Phys. Chem.* 92:312–18
196. Lehmann KK, Coy SL. 1985. *J. Chem. Phys.* 83:3290–96
197. Coy SL, Lehmann KK, DeLucia FC. 1986. *J. Chem. Phys.* 85:4297–303
198. Lehmann KK, Coy SL. 1988. *Ber. Bunsenges. Phys. Chem.* 92:306–11
199. Hardwick JL. 1985. *J. Mol. Spectrosc.* 109:85–98
200. Smalley RE, Wharton L, Levy DH. 1975. *J. Chem. Phys.* 63:4977–89
201. Delon A, Jost R. 1991. *J. Chem. Phys.* 95:5686–700
202. Delon A, Jost R. 1991. *J. Chem. Phys.* 95:5701–18
203. Delon A, Dupre P, Jost R. 1993. *J. Chem. Phys.* 99:9482–95
204a. Georges R, Delon A, Jost R. 1995. *J. Chem. Phys.* 103:1732–54
204b. Delon A, Jost R. 1996. *Faraday Discuss. Chem. Soc.* 102:In press
205. Ionov SI, Davis HF, Mikhaylichenko K, Valachovic L, Beaudet RA, Wittig C. 1994. *J. Chem. Phys.* 101:4809–18
206. Miyawaki J, Yamanouchi K, Tsuchiya S. 1994. *J. Chem. Phys.* 101:4505–13
207. Klippenstein SJ, Radivoyevitch T. 1993. *J. Chem. Phys.* 99:3644–53
208. Tramer A, Voltz R. 1979. In *Excited States*, ed. EC Lim, Vol. 4. New York: Academic
209. Peskin U, Reisler H, Miller WH. 1994. *J. Chem. Phys.* 101:9672–80
210. Peskin U, Miller WH, Reisler H. 1995. *J. Chem. Phys.* 102:8874–86
211. Someda K, Nakamura H, Mies FH. 1994. *Chem. Phys.* 187:195–219
212. Levine RD. 1988. *Ber. Bunsenges. Phys. Chem.* 92:222–27
213. Miller WH, Hernandez R, Moore CB, Polik WF. 1990. *J. Chem. Phys.* 93:5657–66
214. Hernandez R, Miller WH, Moore CB, Polik WF. 1993. *J. Chem. Phys.* 99:950–62
215. Troe J. 1995. *Chem. Phys.* 190:381–92
216. Harding L. 1994. Private communication
217. Troe J. 1983. *J. Chem. Phys.* 79:6017–29
218. Baer T, Hase WL. 1995. *Unimolecular Reaction Dynamics: Theory and Experiments.* Oxford: Oxford Univ.
219. Wardlaw DM, Marcus RA. 1988. *Adv. Chem. Phys.* 70:231–63
220. Marcus R. 1990. *Philos. Trans R. Soc. London Ser. A* 332:283–96
221. Pechukas P, Light JC, Rankin C. 1966. *J. Chem. Phys.* 44:794–805
222. Pechukas P, Light JC. 1965. *J. Chem. Phys.* 42:3281–91
223. Light JC. 1967. *Discuss. Faraday Soc.* 44:14–29
224. Quack M, Troe J. 1974. *Ber. Bunsenges. Phys. Chem.* 78:240–51
225. Quack M, Troe J. 1974. *Ber. Bunsenges. Phys. Chem.* 79:171–79
226. Quack M, Troe J. 1975. *Ber. Bunsenges. Phys. Chem.* 79:469–77
227. Quack M, Troe J. 1977. *Ber. Bunsenges. Phys. Chem.* 81:329–36
228a. Troe J. 1977. *J. Chem. Phys.* 66:4745–57
228b. Troe J. 1977. *J. Chem. Phys.* 66:4758–75
229. Troe J. 1981. *J. Chem. Phys.* 75:226–37
230. Troe J. 1979. *J. Phys. Chem.* 83:114–26